Clustering of settling microswimmers in turbulence

Jingran Qiu[1], Zhiwen Cui[1], Eric Climent[2], and Lihao Zhao[1,3]

[1]AML, Department of Engineering Mechanics, Tsinghua University, 100084 Beijing, China
[2]Institut de Mécanique des Fluides de Toulouse (IMFT), UMR5502 Université de Toulouse, CNRS. Allée du Prof. Camille Soula 31400 Toulouse, France
[3]Laboratory of Flexible Electronics Technology, Tsinghua University, Beijing 100084, China

Correspondence: Lihao Zhao (zhaolihao@mail.tsinghua.edu.cn)

Abstract. Clustering of plankton plays a vital role in several biological activities including feeding, predation and mating. Gyrotaxis is one of the mechanisms that induces clustering. A recent study (Candelier et al., 2022) reported a fluid inertial torque acting on a spherical micro-swimmer, which ~~is analogous to~~ has the same effect as a gyrotactic torque. In this study, we model plankton cells as micro-swimmers that are subject to gravitational sedimentation as well as a fluid inertial torque. We use direct numerical simulations to obtain the trajectories of swimmers in homogeneous isotropic turbulence, and investigate their clustering by Voronoï analysis. Our findings indicate that fluid inertial torque leads to notable clustering, with its intensity depending on the swimming and settling speeds of swimmers. By Voronoï analysis, we demonstrate that swimmers preferentially sample downwelling regions where clustering is more prevalent.

1 Introduction

Plankton are known to form small scale clusters in turbulent environment (Rothschild and Osborn, 1988). These clusters can be down to centimeter-scale and significantly impact basic life processes of plankton such as feeding, predation and mating. Gyrotaxis is one of the mechanisms that causes plankton to form clusters. Many plankton species experience a gravitational stabilizing torque that ~~cause~~ causes them to swim against gravity (Kessler, 1986). When plankton encounter flow shear, the gyrotactic torque opposes the fluid viscous torque and tends to stabilize the swimming direction of the plankton (Qiu et al., 2022b).

Gyrotactic plankton can form different kinds of clusters depending on the flow characteristics. For instance, plankton accumulate in the center or the wall regions in downward or upward pipe flow, respectively (Kessler, 1985). Plankton that are vertical migrating also form clustering when they encounter a shear layer that interrupts the migration (Durham et al., 2009). Plankton in turbulence form small scale clusters that can be characterized by the swimming speed and the intensity of gyrotactic torque. Durham et al. (2013) modeled plankton as spherical gyrotactic micro-swimmers and numerically studied their fractal clustering in homogeneous isotropic turbulence. They demonstrated that the intensity of clustering depends on the

swimming speed and the intensity of gyrotaxis. Clustering is also shown to be correlated to the preferential sampling of downwelling regions (Durham et al., 2013). Later, Zhan et al. (2014) numerically investigated the effect of plankton shape on the clustering. Elongated swimmers are more sensitive to fluid shear than spherical ones, weakening the clustering of strongly gyrotactic swimmers. However, elongation causes preferential alignment in local fluid structures, strengthening the clustering of weakly gyrotactic swimmers. To further clarify the complex relationship between clustering and the swimming speed, gyrotaxis and shape of the swimmers, Gustavsson et al. (2016); Fouxon and Leshansky (2015) established the theory of cluster using stochastic models. These theories were later verified by direct numerical simulations of swimmers in homogeneous isotropic turbulence (Borgnino et al., 2018).

Previous studies suggested that gyrotaxis originates from the asymmetric body structures, such as nonuniform mass distribution (bottom-heaviness) (Kessler, 1985, 1986; Pedley and Kessler, 1987). However, a recent study by Candelier et al. (2022) modeled planktonic microorganisms as settling spherical squirmers and found that a fluid inertial torque drives the squirmer to swim against gravity. The squirmer model is proposed by Lighthill (1952) and improved by Blake (1971) to describe the slip velocity on the surface of microorganisms generated by the movement of cilia. The squirmer model can describe the typical propulsion modes such as puller for algae and pusher for *E. coli* by changing model parameters. Both theory and simulations indicated that fluid inertial torque on a settling squirmer is analogous to a gyrotactic torque, with a magnitude that is proportional to the settling and swimming speeds (Candelier et al., 2022). Planktonic organisms are usually slightly negatively buoyant, thus subject to a gravitational settling effect. For instance, dinoflagellates have a typical swimming speed of $300\ \mu\mathrm{m/s}$ and settling speed of $30\ \mu\mathrm{m/s}$ (Smayda, 2010). Larger organisms such as copepod nauplii have swimming speeds up to $1000\ \mu\mathrm{m/s}$ and settling speeds of $200\ \mu\mathrm{m/s}$ (Titelman and Kiørboe, 2003). As pointed out by Candelier et al. (2022), an organism with large swimming and settling speeds obtain a fluid inertial torque that is comparable to typical gyrotactic torque. However, earlier studies usually neglected the gravity sedimentation and the fluid inertial torque, highlighting the need to consider their effects on the motion of swimming, settling plankton.

In this study, we aim to analyze the clustering of planktonic swimmers under the influence of fluid inertial torque. We model plankton as point-like spherical micro-swimmers undergoing gravity sedimentation. We use direct numerical simulations of swimmer trajectories in homogeneous isotropic turbulence to analyze their clustering characteristic. In section 2.1, we describe the model and the numerical approaches. In section 3, we investigate the clustering using Voronoï analysis and show the relation between clustering and preferential sampling of downwelling regions. In section 4, we draw the conclusions of the present study.

2 Methods

2.1 Model of spherical swimmers

In the present study, we consider a spherical swimmer undergoing gravitational sedimentation as shown in Figure 1. The motion of plankton in fluid flows is usually described by a micro-swimmer model (Durham et al., 2009, 2013; Gustavsson et al., 2016; Lovecchio et al., 2019; Zhan et al., 2014), which assumes a plankton to be a point-like micro-swimmer carried by a fluid flow.

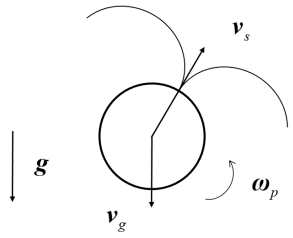

Figure 1. A sketch of a settling swimmer.

~~This assumption is justified when the Reynolds number, $\mathrm{Re} = a|\boldsymbol{v}-\boldsymbol{u}|/\gamma$, is much smaller than unity. Here, the Reynolds number is defin~~

This assumption is justified when the Reynolds number, $\mathrm{Re} = a|\boldsymbol{v}-\boldsymbol{u}|/\gamma$, is much smaller than unity. Here, the Reynolds number is defined based on the radius of a swimmer, a, the differences between the velocities of a swimmer $\boldsymbol{v}$ and the local undisturbed flow $\boldsymbol{u}$, and the kinematic viscosity of the fluid γ. For typical plankton species, this assumption is justified because of their tiny size and limited motility, as summarized in our recent publication (Qiu et al., 2022a). For instance, the typical size and swimming speed of zooplankton are $a = 0.1$ mm and $|\boldsymbol{v}-\boldsymbol{u}| = 1.0$ mm, respectively. Accordingly, we obtain $\mathrm{Re} = 0.1$ using the viscosity of water $\gamma = 10^{-6}$ mm^2/s.

The dynamics of the swimmer is governed by

$$m_p \frac{\mathrm{d}\boldsymbol{v}}{\mathrm{d}t} = 6\pi a\gamma\rho_f(\boldsymbol{u}-\boldsymbol{v}) + m_p(1-\frac{\rho_f}{\rho_p})\boldsymbol{g} + F_s\boldsymbol{n} \tag{1}$$

$$m_p I_p \frac{\mathrm{d}\boldsymbol{\omega}_p}{\mathrm{d}t} = 6\pi a\rho_f\gamma C\left(\frac{1}{2}\boldsymbol{\omega}-\boldsymbol{\omega}_p\right) + \frac{9m_p\rho_f}{8\rho_p}\left[(\boldsymbol{v}-\boldsymbol{u})\times\boldsymbol{v}_s\right], \tag{2}$$

where m_p and ρ_p are the mass and the density of the swimmer, respectively. Eq. (1) governs the translational motion of the swimmer, where the first term on the right-hand-side denotes the Stokes drag. Here, ρ_f is the density of fluid. The second term represents the ~~gravity force~~ gravity and buoyancy on the swimmers due to gravity acceleration $\boldsymbol{g}$. The third term represents a swimming force F_s in the direction of the head of swimmer, denoted as $\boldsymbol{n}$. Meanwhile, Eq. (2) governs the rotation of the swimmer, where $I_p = 2a^2/5$ denotes the moment of inertia per unit mass, and $\boldsymbol{\omega}_p$ represents the angular velocity of the swimmer. The first term on the right-hand-side of Eq. (2) represents the Jeffery torque (Jeffery, 1922), where $C = 4a^2/3$, and $\boldsymbol{\omega}$ is the vorticity of the fluid flow. The second term represents the fluid inertial torque experienced by a squirmer (Candelier et al., 2022), where $\boldsymbol{v}_s$ represents the swimming speed of the squirmer in a quiescent fluid. ~~The model of fluid inertial torque is derived in the limit of $\mathrm{Re} \to 0$, but it has been shown to be justified when $\mathrm{Re} < 0.3$ (Candelier et al., 2~~

The model of fluid inertial torque is derived in the limit of $\mathrm{Re} \to 0$, but it has been shown to be justified when $\mathrm{Re} < 0.3$ (Candelier et al., 2022), within the typical range of plankton physical properties (Qiu et al., 2022a).

Using a velocity and a timescale of the flow u_f and τ_f, we make Eqs. (1) and (2) dimensionless,

$$St\mathrm{St}\frac{\mathrm{d}\boldsymbol{v}'}{\mathrm{d}t'} = \boldsymbol{u}'-\boldsymbol{v}'+\Phi_s\boldsymbol{n}+\Phi_g\boldsymbol{e}_g, \tag{3}$$

$$St\mathrm{St}\frac{I_p}{C}\frac{\mathrm{d}\boldsymbol{\omega}_p'}{\mathrm{d}t'} = \frac{1}{2}\boldsymbol{\omega}'-\boldsymbol{\omega}_p'+\frac{3\tau_f u_f^2}{16\gamma}\left[(\boldsymbol{u}'-\boldsymbol{v}')\times\Phi_s\boldsymbol{n}\right], \tag{4}$$

where the quantities with primes are dimensionless. In above equations, the Stokes number ~~$St = (2a^2\rho_p)/(9\gamma\rho_f\tau_f)$~~ $\mathrm{St} = (2a^2\rho_p)/(9\gamma\rho_f\tau_f)$ reflects the inertia of the swimmer relative to the fluid of the same mass. $\Phi_s = v_s/u_f$ and ~~$\Phi_g = 2(\rho_p/\rho_f - 1)a^2g/(9\gamma u_f)$~~ $\Phi_g = 2(\rho_p/\rho_f - 1)a^2g/(9\gamma u_f)$ are the dimensionless swimming and settling speeds, respectively. ~~Typically, St of planktonic microswimm~~ Typically, St of planktonic microswimmers are usually negligibly small as summarized in Qiu et al. (2022a). For instance, using $a = 0.1\mathrm{mm}$, $\rho_p/\rho_f = 1.05$, and using typical range of turbulence Kolmogorov timescale $\tau_f = 31.6$ to 1.0 s calculated from typical dissipation rate (Kiørboe and Enric, 1995), one obtains $\mathrm{St} = 1.0 \times 10^{-4}$ to 2.3×10^{-3}. In such limit, the left-hand-side of dynamics (3) and (4) can be neglected, and the dynamics simplifies

$$\frac{\mathrm{d}\boldsymbol{x}'}{\mathrm{d}t'} = \boldsymbol{v}', \tag{5}$$

$$\frac{\mathrm{d}\boldsymbol{n}}{\mathrm{d}t'} = \boldsymbol{\omega}_p' \times \boldsymbol{n}, \tag{6}$$

$$\boldsymbol{v}' = \boldsymbol{u}' + \Phi_s\boldsymbol{n} + \Phi_g\boldsymbol{e}_g, \tag{7}$$

$$\boldsymbol{\omega}_p' = \frac{1}{2}\boldsymbol{\omega}' + \frac{1}{2\Psi_I}(\boldsymbol{e}_g \times \boldsymbol{n}). \tag{8}$$

where $\Psi_I = 8\gamma/(3\tau_f u_f^2 \Phi_s \Phi_g)$. ~~The last term of Eq. (8) indicates that fluid inertial torque drives a squirmer swimmer to swim against grav~~ The last term of Eq. (8) indicates that fluid inertial torque drives a squirmer swimmer to swim against gravity. Here, we use a dimensionless timescale Ψ_I to quantify the effect of fluid inertial torque. Ψ_I can be understood as the dimensionless time that a swimmer in still fluid restores upward orientation from an inclined orientation under a reorientation torque. This is identical to the gyrotactic effect induced by bottom-heaviness, which is typically expressed as $(2\Psi)^{-1}(\boldsymbol{e}_g \times \boldsymbol{n})$ (Kessler, 1986). We note that, however, they are two different mechanisms. The gyrotatic torque on a bottom-heaviness cell depends on the distance of the offset between the center of gravity and hydrodynamic forces on a cell, which is usually determined by morphology. On the contrary, the fluid inertial torque is due to the fluid motion disturbed by the swimming and settling behavior of the cell, and thus, determined by motility.

In turbulence, we can take the turbulence Kolmogorov velocity and timescales u_η and τ_η as the characteristic scales of the flow. Using the relation $\gamma = u_\eta^2\tau_\eta$, Ψ_I can be simplified as

$$\Psi_I = \frac{8}{3\Phi_s\Phi_g}. \tag{9}$$

The typical value of Φ_s and Φ_g of plankton can be estimated with their swimming and settling speeds as well as the Kolmogorov velocity scale of ocean turbulence. As summarized in Qiu et al. (2022a), the swimming speeds of different species vary from 200 to 1500 $\mu\mathrm{m/s}$, and the settling speeds vary from 10 to 200 $\mu\mathrm{m/s}$. The Kolmogorov velocity scale of ocean turbulence can be estimated from the typical dissipation rate $\epsilon = 10^{-9}$ to $10^{-6}\mathrm{m^2s^{-3}}$ (Kiørboe and Enric, 1995), yielding $u_\eta = (\gamma\epsilon)^{1/4} = 178$ to $1000\ \mu\mathrm{m/s}$ with $\gamma = 10^{-6}\ \mathrm{m^2s^{-1}}$. Based on these estimations, we consider ~~the~~ a typical parameter space of $0 < \Phi_s < 10$ and $0 < \Phi_g < 1$. ~~Large Φ_s and Φ_g are reached by swimmers with strong motility in weak turbulence which u_η is small. In such case, the a~~ Large Φ_s and Φ_g are reached by swimmers with strong motility in weak turbulence which u_η is small. In such case, the assumptions of our model are still justified. First, Re can be still small even for plankton that swim fast as long as their size is

sufficiently small. Second, St is independent of plankton's motility, which has been shown to be negligibly small for typical turbulence conditions in the ocean (Qiu et al., 2022a).

2.1.1 Direct numerical simulations of swimmers in turbulence

The motion of swimmers in homogeneous isotropic turbulence is simulated by an Eulerian-Lagrangian direct simulations. The flow field is resolved in the Eulerian frame, while the motions of individual swimmers are solved along the Lagrangian trajectories using local flow information at swimmers' positions. The incompressible turbulent flow is directly simulated by solving the Navier-Stokes equations:

$$\frac{\partial \boldsymbol{u}}{\partial t} + \boldsymbol{u} \cdot \nabla \boldsymbol{u} = -\frac{\nabla p_{\mathrm{f}}}{\rho_f} + \gamma \nabla^2 \boldsymbol{u} + \boldsymbol{f}, \tag{10}$$

$$\nabla \cdot \boldsymbol{u} = 0, \tag{11}$$

where p_{f} is the pressure of fluid. An external force $\boldsymbol{f}$ is applied to sustain turbulence and balance the rate of viscous dissipation at the Kolmogorov scale η. The force is applied to the large scale motion using the scheme proposed by Machiels (1997). Periodic boundary conditions are applied on all boundaries of the cubic domain with a size of $(2\pi)^3$. We use pseudo-spectral method to solve the Navier-Stokes equations, and we adopt the 3/2 rule for reducing the aliasing error on the nonlinear term. The separation between turbulent motion of large and small scales is quantified by the Taylor-Reynolds number $\mathrm{Re}_\lambda = u_{\mathrm{rms}} L_\lambda / \gamma$, where u_{rms} is the root-mean-square velocity, and $L_\lambda = u_{\mathrm{rms}} \sqrt{15 \gamma \epsilon^{-1}}$. In the present study, we consider a turbulence of $\mathrm{Re}_\lambda = 60$. To resolve the turbulent flow down to the Kolmogorov scale, we use 96^3 grid points, which allows a maximum wave number resolved to be 1.78 times greater than the Kolmogorov wave number to ensure the accuracy of resolution even at Kolmogorov scales (Pope, 2000). The initial flow field is set as a random flow with an exponential energy spectrum, and an explicit second-order Adams-Bashforth scheme is used for time integration of Eqs. (10) and (11) with a time step smaller than $0.01\tau_\eta$ (Rogallo, 1981).

Swimmers are initialized with random positions and orientations after turbulence is fully developed. When solving the trajectories of swimmer, fluid velocity and its gradients at Eulerian grid points are interpolated by a second-order Lagrangian method at the positions of swimmers. Eqs. (5) and (6) are integrated ~~by~~ using the same second-order Adams-Bashforth scheme as the fluid phase. For each parameter configuration, 10^5 swimmers are simulated, and the statistics are obtained by making an ensemble average over more than 80 uncorrelated time samples after the dynamics has reached a steady state.

3 Results

The instantaneous location and orientation of swimmers are depicted in Figure 2. When swimmers are not settling (Figure 2a), they are distributed randomly with random orientation. Spherical swimmers are known to exhibit random orientation due to the random fluid vorticity of turbulence. As a result, their motions in turbulence remain random, and no cluster is formed. However, when swimmers are settling under the influence of the gravity (Figure 2b), they tend to swim upwards and

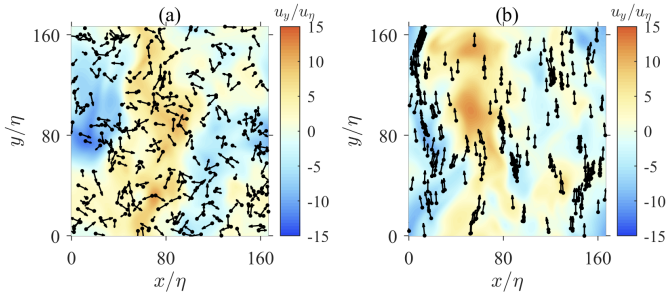

Figure 2. Instantaneous spatial distribution of swimmers in homogeneous isotropic turbulence. Black dots and tiny arrows represent the position and swimming direction of each swimmer, respectively. Background contour represents the vertical fluid velocity u_y. (a) Non-settling swimmers ($\Phi_g = 0,\ \Phi_s = 10$). (b) Settling swimmers ($\Phi_g = 1,\ \Phi_s = 10$).

form clusters due to the contribution of fluid inertial torque~~as predicted by Candelier et al. (2022)~~. As discussed earlier, the fluid inertial torque on a settling swimmer induces ~~an effect similar to gyrotaxis mechanism~~an effect equivalent to gyrotaxis mechanism. Gyrotactic swimmers are known to form spatial clusters and preferentially sample regions with downwelling or upwelling fluid velocity. Previous studies have documented that these phenomena depend on the swimming speed, reorientation time, and the shape of swimmers (Durham et al., 2013; Zhan et al., 2014; Gustavsson et al., 2016; Borgnino et al., 2018). ~~However, in these studies, the reorientation time is determined by bottom-heaviness, which is independent of either swimming or settling~~ However, in these studies, the reorientation time is determined by bottom-heaviness, which is independent of either swimming or settling speeds. Here, a reorientation effect is induced by fluid inertial torque with a timescale Ψ_I, which depends on the swimming and settling speeds of swimmers. Ψ_I cannot be treated as an independent parameter as earlier studies did (Durham et al., 2013; Zhan et al., 2014; Gustavsson et al., 2016; Borgnino et al., 2018). Hence, the picture of clustering may differ from previous studies, and it is worth a further investigation.

3.1 Clustering

The clustering of swimmers is quantified by a three-dimensional Voronoï tessellation (Nilsen et al., 2013; Monchaux et al., 2010). The whole domain is divided into many Voronoï polyhedrons based on the positions of swimmers, with each polyhedron containing one swimmer. Any point in a polyhedron is closest to the corresponding swimmer among all swimmers. The volume of a Voronoï polyhedron is smaller when the corresponding swimmer is surrounded by more other swimmers, and vice versa. Therefore, the distribution of Voronoï polyhedron volumes quantifies the clusters of swimmers.

We use the MATLAB toolbox 'voronoi.m' and 'convhull.m' to compute the vertices of Voronoï polyhedrons and calculate their volumes. Figure 3(a) shows the probability distribution function (PDF) of Voronoï volumes for swimmers with different settling speeds. The PDF of Voronoï volumes of non-settling swimmers remains the same as the one generated from random positions, indicating the absence of clustering. When settling speed increases, the PDFs becomes skewed and a peak at small $V/\langle V\rangle$ appears. This indicates the occurrence of clustering, because swimmers in clusters remain close to each other and their

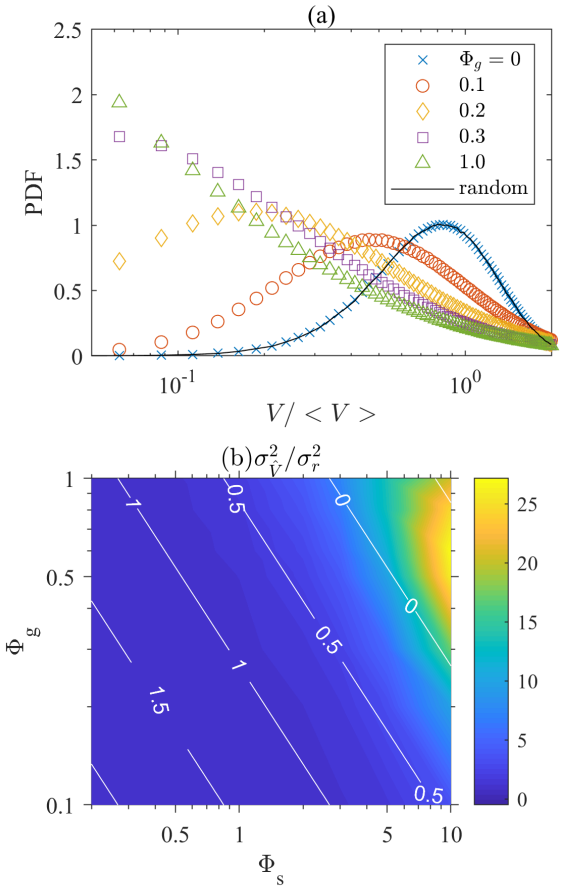

Figure 3. (a) Probability distribution function (PDF) of the volumes of Voronoï cells, normalized by the mean volume $\langle V \rangle$. $\Phi_s = 10$. (b) Variance of Voronoï volumes $\sigma^2_{\hat{V}} = E(V/\langle V \rangle - 1)^2$ normalized by the value of randomly distributed particles. The white contour lines represent the value of $\log_{10} \Psi_I$ in the parameter space.

Voronoï volumes are thus small. Settling swimmers form clusters due to the effect of fluid inertial torque. As shown in Eq. (8), the fluid inertial torque drives settling swimmer to orientate upward with a finite reorientation timescale Ψ_I. This is ~~analogous to~~ the same as the effect of bottom-heaviness (Kessler, 1986) ~~,~~ which also drives swimmers to orientate upward with a timescale Ψ dependent on the offset of the center of gravity with the center of hydrodynamic forces. For inertial torque, however, the timescale Ψ_I is inversely proportional to both the settling and swimming speeds of the swimmer.

To show how clustering depends on the settling and swimming speeds, in Figure 3(b) we depict the variance of Voronoï volumes for different Φ_g and Φ_s. The corresponding magnitude of $\log_{10}\Psi_I$ is also shown by white contour lines. ~~We calculate the Voronoï volu~~ We calculate the Voronoï volume of each swimmer, and obtain the variance of volume distribution normalized by the mean volume of each swimmer, $\sigma_V^2 = E(V/\langle V\rangle - 1)^2$. The variance of Voronoï volumes quantifies the intensity of clustering because a stronger clustering results in a ~~more nonuniform~~ less uniform distribution of Voronoï volumes with larger variance. ~~The results show~~ Figure 3(b) shows that clustering becomes stronger with increasing Φ_s and Φ_g, and reaches a peak at $\Phi_g \approx 0.5$ and $\Phi_s \approx 10$. Further increasing Φ_g leads to a drop of the clustering intensity. This trend can be ~~explain~~ explained using the dimensionless reorientation timescale Ψ_I, which is inversely proportional to Φ_s and Φ_g (Eq. 9). When Ψ_I is zero, gyrotaxis is infinitely strong, causing swimmers to swim straight up against gravity, yielding $\boldsymbol{n} = -\boldsymbol{e}_g$. Since the fluid is incompressible, according to Eq. (7), the velocity field of swimmers has zero divergence, $\nabla \cdot \boldsymbol{v} = \nabla \cdot \boldsymbol{u} = 0$, indicating that no clustering is formed. When Ψ_I is infinitely large, the fluid inertial torque is negligible, and the swimming direction is entirely determined by turbulent shear and becomes random, resulting in no clustering. Therefore, the maximal clustering is expected to occur at a finite Ψ_I. Durham et al. (2013) observed that intensity of clustering of gyrotactic swimmers reaches its maximal when Ψ is of the order of unity (Durham et al., 2013). Since Ψ_I is analogous to Ψ, the maximal clustering in the present case is also observed at certain Φ_s and Φ_g that yields $\Psi_I \sim 1$.

3.2 Preferential sampling of downwelling regions

The clustering of spherical gyrotactic swimmers in turbulence has been shown to be associated with preferential sampling of downwelling regions (Durham et al., 2013). Figure 4 shows the mean vertical fluid velocity at the position of swimmers. Swimmers always sample downwelling regions, and the maximal sampling occurs at large Φ_s but moderate Φ_g which yields ~~$\Psi_I \approx 1.0$~~$\Psi_I \approx 1$. This observation ~~is similar to~~ clearly agrees with Durham et al. (2013) where the maximal preferential sampling is also reached when $\Psi \approx 1$.

Comparing Figure 4 and Figure 3(b), we observed a very similar trend between the sampling of downwelling regions and the intensity of clustering. The magnitude of both quantities increase with Φ_s and reach their maximal at a large Φ_s and a moderate Φ_g. This supports the theory that clustering occurs in downwelling regions (Durham et al., 2013; Fouxon and Leshansky, 2015; Gustavsson et al., 2016). Durham et al. (2013) showed that the divergence of the swimmer velocity field $\nabla \cdot \boldsymbol{v} \propto -\nabla^2 u_y$. Since the $\nabla^2 u_y$ is negatively correlated to u_y in incompressible, homogeneous isotropic turbulence, the sinks of swimmer velocity field tend to be located in downwelling regions with $u_y < 0$. Here, we provide more direct evidence for the clustering in downwelling regions.

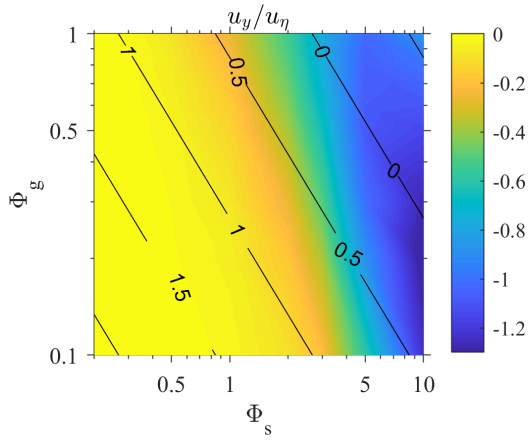

Figure 4. (a) Mean vertical fluid velocity at swimmers positions, $\langle u_y \rangle$, normalized by u_η as a function of Φ_g and Φ_s. The black contour lines represent the value of $\log_{10} \Psi_I$ in the parameter space.

Voronoï analysis allows us to track the Voronoï volume of each swimmer. Based on the values of volumes, we can distinguish whether each swimmer is inside a cluster (with small Voronoï volume) or ~~moving alone away~~ located away from other swimmers (with large Voronoï volume). Figure 5 shows the joint probability distribution function (joint PDF) of u_y and $\log(V/\langle V \rangle)$ for swimmers with different settling speeds. When $\Phi_g = 0$ (Figure 5(a)), fluid inertial torque vanishes and swimmers do not preferentially sample downwelling regions, resulting in a symmetric joint PDF with respect to $u_y = 0$. Moreover, because non-settling swimmers do not form clusters and their Voronoï volumes tend to be uniformed, the joint PDF along $\log(V/\langle V \rangle)$ is concentrated at the peak. However, when $\Phi_g > 0$, the joint PDF becomes asymmetric with respect to u_y (Figure 5(b)). The peak shifts towards $u_y < 0$ because swimmers preferentially sample downwelling regions. Moreover, $\log(V/\langle V \rangle)$ tends to be smaller when $u_y < 0$, indicating that swimmers in downwelling regions are more likely to form clusters. When settling speed increases to $\Phi_g = 0.5$ (Figure 5(c)), the joint PDF becomes flattened along $\log(V/\langle V \rangle)$, because the intensity of clustering reaches its maximal (see Figure 3(b)), making it more probable for swimmers to have both smaller and larger Voronoï volumes. Furthermore, the joint PDF becomes less asymmetric with respect to u_y, indicating that strong clustering no longer occurs only in downwelling regions. When Φ_g further increases to $\Phi_g = 1$, the distribution becomes slightly concentrated again because the intensity of clustering is weakened compared to the case of $\Phi_g = 0.5$. In general, the joint PDFs reveal that swimmers are more likely to form cluster in downwelling regions, but when clustering is intense, the bias is weak.

4 Conclusions

A settling spherical squirmer experiences a fluid inertial torque that causes it to swim against gravity, acting as an effective gyrotactic torque (Candelier et al., 2022). While previous studies have focused on gyrotactic torque originating from bottom-heaviness, the role of fluid inertial torque has been neglected (Durham et al., 2013; Zhan et al., 2014; Gustavsson et al., 2016;

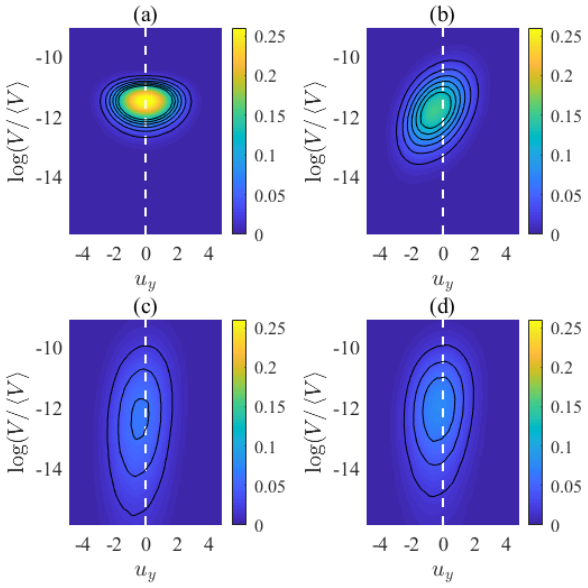

Figure 5. Joint probability distribution function (PDF) of vertical fluid velocity u_y and the Voronoï volumes $\log(V/\langle V\rangle)$. $\Phi_s = 10$ for all panels. White dashed lines correspond to $u_y = 0$. (a) $\Phi_g = 0$. (b) $\Phi_g = 0.2$. (c) $\Phi_g = 0.5$. (d) $\Phi_g = 1.0$.

Borgnino et al., 2018). In the present study, we modeled the inertia-less micro-swimmer under the influence of fluid inertial torque. The magnitude of the torque is quantified using a dimensionless reorientation timescale Ψ_I which is proportional to the inverse of dimensionless swimming speed (Φ_s) and settling speed (Φ_g).

Using direct numerical simulation, we investigated the clustering of swimmers under fluid inertial torque. We quantified the clustering using a Voronoï analysis. When swimmers are not settling, the fluid inertial torque vanishes, and the swimmers are randomly distributed resulting from a random direction of swimming, with no clustering observed. Settling swimmers experience a fluid inertial torque and behave similarly to gyrotactic swimmers. We observed that swimmers form more intense clustering when Φ_s and Φ_g become larger, with maximal clustering intensity occurring at the largest Φ_s and a modest Φ_g, corresponding to $\Psi_I \sim 1$.

We also examined how the clustering of spherical swimmers is related to their preferential sampling of downwelling regions. We found that when swimmers are not settling, their dynamics remains isotropic, and no preferential sampling is observed in the gravity direction. However, the fluid inertial torque, as well as the settling speed, break this symmetry, and drive settling swimmers to sample downwelling regions. The sampling is more pronounced with larger Φ_s and Φ_g, reaching the maximum when $\Psi_I \approx 1$. The trend of preferential sampling shows a similar pattern to that of clustering intensity, indicating a correlation between the two phenomena. We used the joint PDF of Voronoï volumes and local vertical fluid velocity to demonstrate that swimmers tend to form clusters in downwelling regions.

The fluid inertial torque on settling swimmers can cause the formation of small-scale clusters, highlighting the importance of fluid inertial effects on the dynamics of plankton. However, most of earlier studies did not consider gravitational sedimentation, leading to the neglect of fluid inertial torque. This underestimates the intensity of gyrotaxis because the total gyrotactic torque is contributed by both fluid inertial torque and bottom-heaviness. In addition, the fluid inertial torque is proportional to the swimming and settling speeds, making the reorientation time a dependent parameter. Therefore, planktonic swimmers have the potential to tune their ~~reorientation behavior and thus control clustering intensity~~ reorientation behavior and thus control clustering intensity by adjusting their swimming speed, which ~~might~~ further impact their mating, predation and feeding.

~~We note that the present study considered only spherical swimmers~~Finally, it is necessary to clarify the assumptions of our model. First, Non-spherical plankton, such as elongated ones, probably experience a fluid inertial torque stemming from both their non-spherical shape (Dabade et al., 2015; Sheikh et al., 2020; Gustavsson et al., 2019; Qiu et al., 2022a) and propulsion mechanism (Candelier et al., 2022). While the analytical solution for the fluid inertial torque on a non-spherical swimmer remains unclear, fully resolved numerical simulation could be used to reveal the dynamics of non-spherical settling swimmers. The resulting findings could be potentially applied to the model of point-like swimmer. The second assumption is that we neglected the inertia of the mic

Code and data availability. Raw data from simulation are available upon request to corresponding author.

Author contributions. J.Q., E.C and L.Z. designed the project; J.Q. and L.Z. performed research; J.Q. and Z.C. developed numerical tools; J.Q. analyzed data; J.Q., E.C. and L.Z wrote the paper.

Competing interests. The authors declare no conflict of interest.

Acknowledgements. This work was supported by the National Natural Science Foundation of China (Grant No. 92252104, 12388101 and 92252204). Z.C. acknowledges the support by China Postdoctoral Science Foundation (grant number 2022M721849).

References

Blake, J. R.: A spherical envelope approach to ciliary propulsion, Journal of Fluid Mechanics, 46, 199–208, 1971.

Borgnino, M., Boffetta, G., De Lillo, F., and Cencini, M.: Gyrotactic swimmers in turbulence: shape effects and role of the large-scale flow, Journal of Fluid Mechanics, 856, 2018.

Candelier, F., Qiu, J., Zhao, L., Voth, G., and Mehlig, B.: Inertial Torque on a Squirmer, Journal of Fluid Mechanics, 953, R1, 2022.

Dabade, V., Marath, N. K., and Subramanian, G.: Effects of inertia and viscoelasticity on sedimenting anisotropic particles, Journal of Fluid Mechanics, 778, 133, 2015.

Durham, W. M., Kessler, J. O., and Stocker, R.: Disruption of vertical motility by shear triggers formation of thin phytoplankton layers, Science, 323, 1067–1070, 2009.

Durham, W. M., Climent, E., Barry, M., De Lillo, F., Boffetta, G., Cencini, M., and Stocker, R.: Turbulence drives microscale patches of motile phytoplankton, Nature Communications, 4, 1–7, 2013.

Fouxon, I. and Leshansky, A.: Phytoplankton's motion in turbulent ocean, Physical Review E, 92, 013 017, 2015.

Gustavsson, K., Berglund, F., Jonsson, P. R., and Mehlig, B.: Preferential sampling and small-scale clustering of gyrotactic microswimmers in turbulence, Physical Review Letters, 116, 108 104, 2016.

Gustavsson, K., Sheikh, M. Z., Lopez, D., Naso, A., Pumir, A., and Mehlig, B.: Effect of fluid inertia on the orientation of a small prolate spheroid settling in turbulence, New Journal of Physics, 21, 083 008, 2019.

Jeffery, G. B.: The motion of ellipsoidal particles immersed in a viscous fluid, Proceedings of the Royal Society of London. Series A, 102, 161, 1922.

Kessler, J. O.: Hydrodynamic focusing of motile algal cells, Nature, 313, 218–220, 1985.

Kessler, J. O.: Individual and collective fluid dynamics of swimming cells, Journal of Fluid Mechanics, 173, 191–205, 1986.

Kiørboe, T. and Enric, S.: Planktivorous feeding in calm and turbulent environments, with emphasis on copepods, Marine Ecology Progress Series, 122, 135–145, 1995.

Lighthill, M. J.: On the squirming motion of nearly spherical deformable bodies through liquids at very small Reynolds numbers, Communications on pure and applied mathematics, 5, 109–118, 1952.

Lovecchio, S., Climent, E., Stocker, R., and Durham, W. M.: Chain formation can enhance the vertical migration of phytoplankton through turbulence, Science Advances, 5, 7879, 2019.

Machiels, L.: Predictability of small-scale motion in isotropic fluid turbulence, Physical Review Letters, 79, 3411, 1997.

Monchaux, R., Bourgoin, M., and Cartellier, A.: Preferential concentration of heavy particles: A Voronoï analysis, Physics of Fluids, 22, 103 304, 2010.

Nilsen, C., Andersson, H. I., and Zhao, L.: A Voronoï analysis of preferential concentration in a vertical channel flow, Physics of Fluids, 25, 115 108, 2013.

Pedley, T. J. and Kessler, J.: The orientation of spheroidal microorganisms swimming in a flow field, Proceedings of the Royal Society of London. Series B. Biological Sciences, 231, 47–70, 1987.

Pope, S. B.: Turbulent Flows, Cambridge University Press, Cambridge, UK, 2000.

Qiu, J., Cui, Z., Climent, E., and Zhao, L.: Gyrotactic mechanism induced by fluid inertial torque for settling elongated microswimmers, Physical Review Research, 4, 023 094, 2022a.

Qiu, J., Marchioli, C., and Zhao, L.: A review on gyrotactic swimmers in turbulent flows, Acta Mechanica Sinica, 38, 722 323, 2022b.

Rogallo, R. S.: Numerical experiments in homogeneous turbulence, vol. 81315, National Aeronautics and Space Administration, 1981.

Rothschild, B. and Osborn, T.: Small-scale turbulence and plankton contact rates, Journal of plankton Research, 10, 465–474, 1988.

Sheikh, M. Z., Gustavsson, K., Lopez, D., Lévêque, E., Mehlig, B., Pumir, A., and Naso, A.: Importance of fluid inertia for the orientation of spheroids settling in turbulent flow, Journal of Fluid Mechanics, 886, A9, 2020.

Smayda, T. J.: Adaptations and selection of harmful and other dinoflagellate species in upwelling systems. 2. Motility and migratory behaviour, Progress in Oceanography, 85, 71–91, 2010.

Titelman, J. and Kiørboe, T.: Motility of copepod nauplii and implications for food encounter, Marine Ecology Progress Series, 247, 123–135, 2003.

Zhan, C., Sardina, G., Lushi, E., and Brandt, L.: Accumulation of motile elongated micro-organisms in turbulence, Journal of Fluid Mechanics, 739, 22–36, 2014.